Mon. Not. R. astr. Soc. (1991) **248,** 688–700

Ring formation in triaxial potentials

F. R. Pearce and P. A. Thomas
Astronomy Centre, Sussex University, Falmer, Brighton BN1 9QH

Accepted 1990 September 19. Received 1990 September 17; in original form 1990 June 26

SUMMARY

The formation of rings of gas in the outer regions of early-type galaxies is considered. It has previously been shown that the stable orbital planes lie perpendicular to the major and minor axes. Discs initially inclined in other directions will precess about one of the symmetry axes. The precession rate varies with radius and will thus cause the disc to warp. This induces a local viscosity which acts so as to oppose relative motion and causes the disc to settle into one of the preferred planes. Our simulations show a qualitatively different behaviour: viscosity is insufficient to prevent break-up of the disc and so gas clouds move to fill the available tube orbit. After a few precession times particles have differentially precessed through 180° at a given radius and collisions occur in the symmetry plane of the tube orbit forming a ring *in situ*.

We simulate ring formation following the merger of a small gas-rich (dwarf-spiral) companion. An initial disc of gas forms in the collision plane only if the rotational angular momentum of the companion is approximately aligned with the collision direction; otherwise a ring rapidly forms in one of the stable planes.

Accretion of gas into the core of the host galaxy occurs not only when the disc's angular momentum vector lies close to the symmetry of a near-axisymmetric system but also, more generally, when the gas is able to precess about both the minor and major axis in a triaxial potential.

1 INTRODUCTION

We present a study of gas ring formation in a triaxial potential using an *N*-body code. This work was stimulated by previous studies of 'polar rings' – rings of gas and dust which appear to lie perpendicular to the projected major axis of the underlying galaxy. The best-known example is the Spindle, or Helix Galaxy, NGC 2685 (Schweizer, Whitmore & Rubin 1983, hereafter SWR). There are perhaps a dozen other known examples (Mould *et al.* 1982; Wakamatsu & Arp 1983; Taniguchi, Shibata & Wakamatsu 1986; van Gorkom, Schechter & Kristian 1987; Whitmore, McElroy & Schweizer 1987, hereafter WMS; see also the review by Athanassoula & Bosma 1985). Because of their similarity with barred spirals possessing tightly bound arms, there are no clear-cut examples of face-on polar rings. However, Hoag-type objects which appear to be elliptical galaxies surrounded by circular rings (Hoag 1950; Schweizer *et al.* 1987; Wakamatsu 1990) are one set of possible candidates.

The problem of finding the stable ring geometries in a fixed potential has been discussed by many authors (e.g. Dobrovolski 1980; Tohline, Simonson & Caldwell 1982; Steiman-Cameron & Durisen 1982, hereafter SD82) and this has been extended by Tohline & Durisen (1982), Durisen *et al.* (1983) and Steiman-Cameron & Durisen (1984) to a tumbling potential. In an axisymmetric potential only discs with their momentum vectors aligned with the symmetry axis are stable. However, in the triaxial potentials discussed here (which have three planes of symmetry) both short- and long-axis rings, with the momentum vector along the minor and major axis, respectively, are possible; intermediate-axis rings are unstable.

Throughout this paper we use the term 'disc' to mean a general annular distribution of gas whereas the term 'ring' is reserved for a disc which has settled into a relatively long-lived configuration in one of the preferred planes. 'Wide' and 'narrow' are used to indicate the radial extent of a disc, while 'thick' and 'thin' indicate height perpendicular to the plane.

Differential precession will occur for a disc not in a stable configuration and the dissipation of relative motion between neighbouring elements of the disc may cause it to settle into a ring. This process has been investigated by Habe & Ikeuchi (1985, hereafter HI85) who simulated the motion of 1000 gas particles with an artificial viscosity to damp out convergent motions of 10 km s^{-1} or more, and by Steiman-Cameron & Durisen (1988, hereafter SD88) who split the

disc up into many narrow annuli with viscosity to damp out relative motion between neighbours. They both concluded that gas discs will indeed settle on to a preferred plane on a time-scale similar to the differential precession time between the inner and outer edge of a test particle's excursion in the disc.

Both of these studies emphasize a picture in which the disc remains continuous, albeit highly warped, and in which local viscosity acts so as to return the disc to a planar configuration. This can only be achieved in one of the stable planes and so the system settles down into a ring. There is a problem with these results, however, in that the viscosity may not be large enough to preserve the continuous nature of the disc. HI85 have to choose a large effective size for their gas clouds (in effect they assume a continuous distribution of gas in the disc), dissipation of particles on neighbouring orbits is only effective for initial inclinations close to one of the preferred planes, and they present no clear example of precession of the disc as a whole. In addition they only consider initially thin and uniformly rotating, narrow discs. SD88 do present results in which a disc initially inclined at 40° to a preferred plane will settle down into a ring but we suggest that they seriously overestimate the viscosity in their model. A cylindrical geometry is assumed for each annulus with the result that neighbouring annuli are taken to be in continuous contact no matter what their orientation. However, differential precession of the order required to give significant viscosity (SD88 fig. 9) will cause particles to move in and out of the plane of the disc as their distance from the centre of the galaxy changes. Even small radial excursions of the order of 5 per cent which are needed in order to couple different parts of the disc will lead to displacements of 2 kpc above and below the plane at a radius of 5 kpc for a disc inclination of 40°. Unless the disc is very thick, therefore, viscosity of this kind will be ineffective except at small inclinations.

In this paper we develop a numerical code in which the gas is treated as a collection of dense clouds rather than a continuous medium. Dissipation is treated in a qualitatively different way from HI85, by inelastic collisions between gas clouds. We confirm that some dissipation of relative motion can be made to occur for discs whose initial inclination angle is small. However, this is only possible for long-range interactions in the disc and even then the disc does not precess as a whole. For more realistic cloud distributions and interaction conditions we find a qualitatively different behaviour; viscosity is insufficient to prevent break-up of the disc and the gas clouds rapidly spread to fill the available tube orbit. After a few precession times collisions occur on the midplane of the tube orbit and a ring forms *in situ*. Ring formation is enhanced by irregularities in the galactic potential and the initial conditions which tend to cause increased differential precession in neighbouring orbits.

As well as discussing the evolution of flat discs we also investigate ring formation from more realistic initial conditions such as may occur during infall of a gas-rich companion. Previous investigations have followed the prescription set out by Shane (1980) who suggested that gas from a disrupted companion would quickly settle down into a cold, flat disc with gas clouds on near-circular orbits lying in or close to the plane of the collision. We find that this is indeed a possibility, but in the more general and more interesting case the infalling gas does not collapse into a plane. Gas clouds are injected on a range of orbits, differential precession is thereby enhanced and ring formation can occur much more rapidly.

In Section 2 we develop our integration scheme and demonstrate its stability for a single particle. We confirm the theoretical results of SD82 and show precession of the momentum vector about both the long and short axes of a triaxial potential. Then we introduce and test two different models for the dissipation of relative cloud motions. The numerical code is applied to the evolution of cold gas discs in Section 3, and Section 4 looks at ring formation from more realistic initial conditions such as might occur from the infall of a gas-rich companion galaxy. Finally, in Section 5, we summarize our results and discuss the implications for the structure of elliptical galaxies.

2 NUMERICAL ALGORITHM

2.1 The potential

Throughout this paper we use the logarithmic potential of HI85. The potential, Φ, at the point $\boldsymbol{r}(x, y, z)$ is

$$\Phi = \Phi_c \ln\left(\frac{x^2}{a^2} + \frac{y^2}{b^2} + \frac{z^2}{c^2} + e\right), \tag{1}$$

where Φ_c is the central value and $a \le b \le c$ are the semi-axes. The constant $e \approx 2.718$ is introduced so as to give a finite core; it is mostly irrelevant for our orbiting particles as $r = \sqrt{\boldsymbol{r}\cdot\boldsymbol{r}} \gg e$. Note that in this regime the equations are independent of r, there being no natural length. We note that this potential can give negative densities at large distances along the minor axis if $1/a^2 > 1/b^2 + 1/c^2$ – this will not be a problem here. Within the code we use units in which a, b and $c \approx 1$ and set $\Phi_c = 1$. To convert to physical units we use a typical length scale of 100 pc and a circular speed (for $a = b = c = 1$) of

$$v_c = \left(r\frac{\partial\Phi}{\partial r}\right)^{1/2} = \sqrt{2} \approx 200 \text{ km s}^{-1}. \tag{2}$$

The equations of motion can easily be determined from the Hamiltonian

$$H = T + \Phi = \tfrac{1}{2}\dot{\boldsymbol{r}}^2 + \Phi \tag{3}$$

$$\ddot{\boldsymbol{r}} = -\nabla\Phi, \tag{4}$$

with a first integral (conservation of energy) $H = E = \text{constant}$.

2.2 Integration scheme

Our integration scheme is a low-order predictor-corrector method (a higher order method is not practicable due to the large number of collisions between particles). The position of the particle is predicted using an Euler scheme:

$$\boldsymbol{r}_p = \boldsymbol{r}(t) + \dot{\boldsymbol{r}}(t)\Delta t \tag{5}$$

and the new acceleration $\ddot{\boldsymbol{r}}_p = -\nabla\Phi(\boldsymbol{r}_p)$ is evaluated. The new velocity and position are then evaluated using the

trapezium rule:

$$\dot{\boldsymbol{r}}(t+\Delta t)=\dot{\boldsymbol{r}}(t)+\tfrac{1}{2}[\ddot{\boldsymbol{r}}(t)+\ddot{\boldsymbol{r}}_{\rm p}]\Delta t \tag{6}$$

$$\boldsymbol{r}(t+\Delta t)=\boldsymbol{r}(t)+\tfrac{1}{2}[\dot{\boldsymbol{r}}(t)+\dot{\boldsymbol{r}}(t+\Delta t)]\Delta t. \tag{7}$$

Initial and final energies are then compared and the step length adjusted until the relative error is less than 1 part in 10^4. Once this has been achieved the velocity is altered to force exact conservation of energy. We must therefore use the modulus of the angular momentum to test the accuracy of our integration and this is conserved to a very high order in an axisymmetric potential (see below).

The complete scheme was tested by reproducing closed orbits in a Keplerian potential. Both circular and highly elliptical orbits are reproduced accurately with a systematic change in angular momentum of less than 1 part in 10^9 per integration step, using 300 steps per orbit.

2.3 Single-particle orbits

In this section we look at the trajectories of particles on near-circular orbits. It is convenient to characterize orbits by their specific angular momentum $\boldsymbol{J}=\boldsymbol{r}\wedge\dot{\boldsymbol{r}}$ which varies slowly in time. $\boldsymbol{J}$ and the rate of change of $\boldsymbol{J}$ are given in the usual spherical polar coordinates by

$$\boldsymbol{J}=\boldsymbol{r}\wedge\dot{\boldsymbol{r}}=(0,\,-r^2\sin\theta\,\dot{\phi},\,r^2\dot{\theta}) \tag{8}$$

$$\dot{\boldsymbol{J}}=\boldsymbol{r}\wedge\ddot{\boldsymbol{r}}=\left(0,\frac{1}{\sin\theta}\frac{\partial H}{\partial\phi},\,-\frac{\partial H}{\partial\theta}\right). \tag{9}$$

The rate of change of the magnitude of J is given by

$$\frac{d(\frac{1}{2}J^2)}{dt}=\boldsymbol{J}\cdot\dot{\boldsymbol{J}}=-r^2\left(\dot{\theta}\frac{\partial H}{\partial\theta}+\dot{\phi}\frac{\partial H}{\partial\phi}\right). \tag{10}$$

Thus J varies over an orbit but for circular motion the secular change in J, averaged over a whole orbit, is zero. In fact J does change slightly as the orbits do not close, but this change again averages to zero over a whole precession period.

We will follow previous authors in treating our triaxial potential as a small perturbation of a spherically symmetric system. To zeroth order we take

$$H_0=T+\Phi_0\left(\frac{r}{A}\right)=T+2\Phi_{\rm c}\ln\left(\frac{r}{A}\right), \tag{11}$$

where $A=[\frac{1}{3}(1/a^2+1/b^2+1/c^2)]^{1/2}$ is an average semi-axis. This unperturbed potential admits stable solutions of constant radius which minimize the energy for a fixed angular momentum. The canonical variables can be expressed in terms of four constants of the motion, the node Ω, inclination i, angular velocity $\dot{\chi}$, and phase χ_0, (see Fig. 1) via the equations

$$\begin{aligned}
&\cos\theta=\sin\chi\sin i\\
&\tan(\phi-\Omega)=\tan\chi\cos i\\
&p_\theta=-\dot{\chi}\cos\chi\sin i/\sqrt{1-\sin^2\chi\sin^2 i}\\
&p_\phi=\dot{\chi}\cos i,
\end{aligned} \tag{12}$$

where

$$\chi=\dot{\chi}t+\chi_0.$$

Next we consider the perturbing potential $\Phi_1(\theta,\phi)$:

$$\Phi_1=\Phi_{\rm c}A^2\left[\sin^2\theta\cos^2\phi\left(\frac{1}{a^2}-\frac{1}{A^2}\right)+\sin^2\theta\sin^2\phi\times\left(\frac{1}{b^2}-\frac{1}{A^2}\right)+\cos^2\theta\left(\frac{1}{c^2}-\frac{1}{A^2}\right)\right]. \tag{13}$$

Circular orbits are no longer possible, however the peculiar acceleration is small and so to first order we can take $r=$ constant. Secular changes take place on a time-scale much longer than the orbital period and so it is convenient to average the potential over one orbit. The details can be found in SD82, HI85 and references therein.

$$\langle\Phi_1\rangle=\Phi_{\rm c}A^2[C_{20}(\tfrac{3}{2}\sin^2 i-1)-3C_{22}\sin^2 i\cos 2\Omega],$$

where

$$C_{20}=-\frac{A^2}{6}\left(\frac{1}{a^2}+\frac{1}{b^2}-\frac{2}{c^2}\right) \tag{14}$$

$$C_{22}=-\frac{A^2}{12}\left(\frac{1}{a^2}-\frac{1}{b^2}\right).$$

By a tedious but straightforward application of canonical perturbation theory (e.g. Goldstein 1980, chapter 11) the rate of change of orbital parameters can be determined. The angular velocity and orbital phase are constant, in agreement with the invariance of J deduced above, while the node and inclination precess at the rates

$$\begin{aligned}
\frac{d\Omega}{dt}&=-\frac{1}{J\sin i}\frac{\partial\langle\Phi_1\rangle}{\partial i}=-\dot{\chi}\cos i(\tfrac{3}{2}C_{20}-3C_{22}\cos 2\Omega)\\
\frac{di}{dt}&=\frac{1}{J\sin i}\frac{\partial\langle\Phi_1\rangle}{\partial\Omega}=\dot{\chi}(3C_{22}\sin i\sin 2\Omega).
\end{aligned} \tag{15}$$

Because the angular velocity is conserved, the trajectory of the angular momentum vector follows the curves $\Phi_1(\theta,\phi)=$ constant and the orbit will precess around either the short or the long axis (see fig. 1 of SD82). The dividing lines between the two cases are great circles through the y-axis and inclined at angle $\pm I$ to the x–y plane, where

$$\sin^2 I=\frac{1/b^2-1/c^2}{1/a^2-1/c^2}. \tag{16}$$

Thus the probability that a random orbit will precess around the minor axis is $2I/\pi$.

We first consider an oblate potential, O1 ($a=0.9$, $b=1.0$, $c=1.0$). The angular momentum in the x-direction, J_x, is theoretically conserved in this case, precessing uniformly around the x-axis with a period $4\pi r/[v_{\rm c}\cos i\,A^2(1/a^2-1/c^2)]$. Departures from spherical symmetry cause J to vary slightly with orbital phase. On the other hand our scheme conserves J_x to 3 parts in 10^6 per orbit (1 part in 10^8 per step) although there is a small systematic drift to lower values. The theoretical precession rate at $i=45°$ is 11.2 orbits per precession

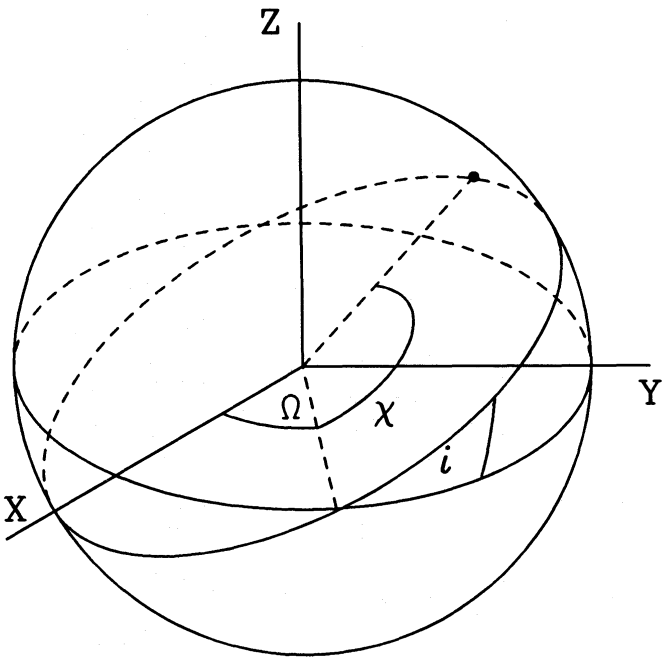

Figure 1. The coordinate system as defined in the text.

time whereas the measured value was 12.3. At a similar inclination model O2 ($a=0.98$, $b=1.0$, $c=1.0$) took 69 orbits to precess once, compared to a predicted value of 68. Thus as the deviation from spherical symmetry decreases the predicted and measured values converge. Prolate potentials (e.g. P1: $a=1.0$, $b=1.0$, $c=1.1$) are similar, except that precession now occurs around the z-axis, and our tests gave equally good results.

Progressing to a triaxial figure, T1 ($a=0.9$, $b=1.0$, $c=1.1$) we can demonstrate precession about either the long or the short axis depending upon the initial alignment of the momentum vector. The change over angle (I above) is 35°.0 which differs somewhat from the theoretical prediction of 40°.7, however, the perturbations from spherical symmetry are now quite large as the expression for I involves differences of the squares of a, b and c. For a less perturbed model, T2 ($a=0.98$, $b=1.0$, $c=1.02$), the change over angle is 43°.0 closer to the predicted angle of 44°.1.

We can classify particle orbits as major- and minor-axis tube orbits depending upon the axis which they precess around (e.g. Binney & Tremaine 1987, p. 155). Each orbit type approximately conserves momentum around the appropriate axis. Near the centre of the potential [$r/A=O(1)$] box orbits are possible and were successfully generated by our code, but these will be of no further concern to us here.

2.4 Many-particle orbits with collisions

The behaviour of a single cloud is modified by interactions with its neighbours – in particular relative motion may be dissipated. The interaction and dissipation rates depend upon the size and mass of the clouds. The effective cross-section of the clouds for tidal dissipation can be estimated as follows. Consider a cloud of radius R and mass M passing another cloud at distance $d \gg R$. Then the tidal acceleration exerted by one of the clouds at the surface of the other is

$$a_{\rm tidal} = \frac{2GMR}{d^3}. \tag{17}$$

The impulsive velocity is $\Delta v = a\Delta t$, with $\Delta t \sim d/v$, where v is the relative velocity of the clouds

$$\Delta v \sim \frac{2GMR}{d^2 v}. \tag{18}$$

Two clouds on circular orbits of radii r and $r+d$, respectively, have a relative orbital velocity $v = dv_c/r$, where v_c is the circular velocity. We will assume that dissipation is 100 per cent efficient so that to get rid of a significant fraction of the relative orbital energy we require $v \sim \Delta v$. This occurs when

$$\left(\frac{d}{r}\right)^4 \sim 2\left(\frac{M}{M_{\rm gal}}\right)\frac{R}{r}, \tag{19}$$

where we have used $v_c^2 = GM_{\rm gal}/r$. We take $M/M_{\rm gal} \sim 10^{-5}$, $r \sim 100$ and $R \sim 0.5$ which leads to $d \sim 1.8$. This cross-section is of the same order as the cloud size and therefore the approximation used to estimate the tidal acceleration breaks down. Nevertheless it motivates the following collision algorithm.

C1. The relative motion of clouds is dissipated if they come into contact during a time-step. Due to the low order of our integration scheme an individual cloud orbit is very closely linear over a single time-step and we therefore assume that the cloud centre follows a linear trajectory; the calculation of the minimum separation of two clouds is then straightforward. The cloud parameters are chosen to match observations of Giant Molecular Clouds in the Milky Way which have typical radii of 50 pc and masses of $10^6\ M_\odot$ (Brinks & Burton 1983). Our calculations are completely independent of M as we ignore cloud–cloud self-gravity and assume $M \ll M_{\rm gal}$. The referee has pointed out that H I clouds are smaller and more numerous and would therefore give more collisions and a greater viscosity (although not necessarily enough to prevent disruption of the disc – see Section 3.4). However, Giant Molecular Clouds if they exist are likely to contain most of the gas mass, they will be dynamically distinct and collisions between them should provoke star formation to light up the ring. As a practical limitation we do not have the resources to model more than 1000 particles.

We have tried two approaches once a collision is flagged. These form the extreme cases of the proposed situation in the Milky Way in which clouds grow by merging until they reach a critical size for star formation and are then broken up by the energy released in supernovae (e.g. Tenorio-Tagle 1990).

C1a. We assume that the colliding clouds stick together to form a single cloud at the centre-of-mass of the original pair, moving so as to conserve momentum. The radius of the final cloud is increased so as to conserve density. This allows very large clouds of up to $10^9\ M_\odot$ to develop as there is no maximum mass.

C1b. We assume that clouds cannot get any larger than their present size. As in *C1a* we form a combined structure at the centre-of-mass but then we immediately break it up by giving each cloud an additional small velocity (1 per cent of the circular velocity) in opposite directions away from the centre-of-mass. The clouds are also given a small separation of $2r_{\rm cloud}$ along this random velocity vector to avoid re-collision at the next step.

With this collision algorithm the mean-free path between collisions is in general quite large (of order one collision per orbit) and the behaviour is qualitatively different from the models of HI85 and SD88. HI85 used an SPH code with a Gaussian smoothing kernel of variance 250 pc which means that relative motions of greater than 10 km s^{-1} are effectively damped on length scales of up to a few times 250 pc. To try to reproduce their results and to investigate the effect of longer range dissipation we also consider a second collision scheme.

C2. To mimic the SPH code we need a very effective dissipation mechanism. This is achieved by having numerous 'collisions'. At the end of each time-step all pairs of clouds which have a decreasing separation less than $d_{\rm sep}$ have their relative velocity reduced to zero, conserving momentum and leaving the cloud positions unaltered. Clouds which are moving apart are left with their velocities unchanged. $d_{\rm sep}$ is typically chosen to be of order a few cloud separations but less than the scale size r of the system.

As well as dissipating relative motion, gravitational interactions between clouds can transform ordered rotational motion into disordered 'thermal' motion. This can have two opposing effects. It will 'puff up' a cold disc, but it can also lead to radial motions which will couple different parts of the disc, thereby aiding solid-body precession. The cross-section for a strong collision is calculated analogously with that for tidal dissipation except that the force is now the Newtonian gravitational attraction. This change leads to

$$\left(\frac{d}{r}\right)^3 \sim \left(\frac{M}{M_{\rm gal}}\right). \tag{20}$$

For $r \sim 100$, and $M/M_{\rm gal} \sim 10^{-5}$, this gives $d \approx 2.15$ which is only slightly greater than the dissipation scalelength. For this reason we choose to ignore gravitational interactions between clouds.

3 DISC EVOLUTION

3.1 Initial conditions

To begin with we look at the evolution of an initially thin, cold disc. This will enable us to compare our results with HI85 and to understand the dissipation mechanism. We use an annulus with inner radius $r_{\rm min} = 50$, outer radius $r_{\rm max} = 100$ and a full thickness $h = 5$, which is manufactured in the x–y plane and then inclined to any desired orientation. In all cases we use 1000 clouds, which for a scalelength of 1 unit = 100 pc corresponds to a total mass of about $10^9\ M_\odot$, typical of many observed polar ring galaxies. The clouds are placed at a radius, r, chosen uniformly between $r_{\rm min}$ and $r_{\rm max}$ with the node and the phase of the initial orbit being picked at random (see Fig. 1). The inclination above the x–y plane is fixed at $\arcsin(h/r)$; thus the initial orbital inclination varies slightly between the inner and outer edges of the disc. The initially random phase of the orbits prevents the disc height collapsing to zero which may be a problem in earlier simulations. The clouds are given an initial tangential velocity of $\sqrt{2}$, equivalent to the circular velocity in a spherically symmetrical potential.

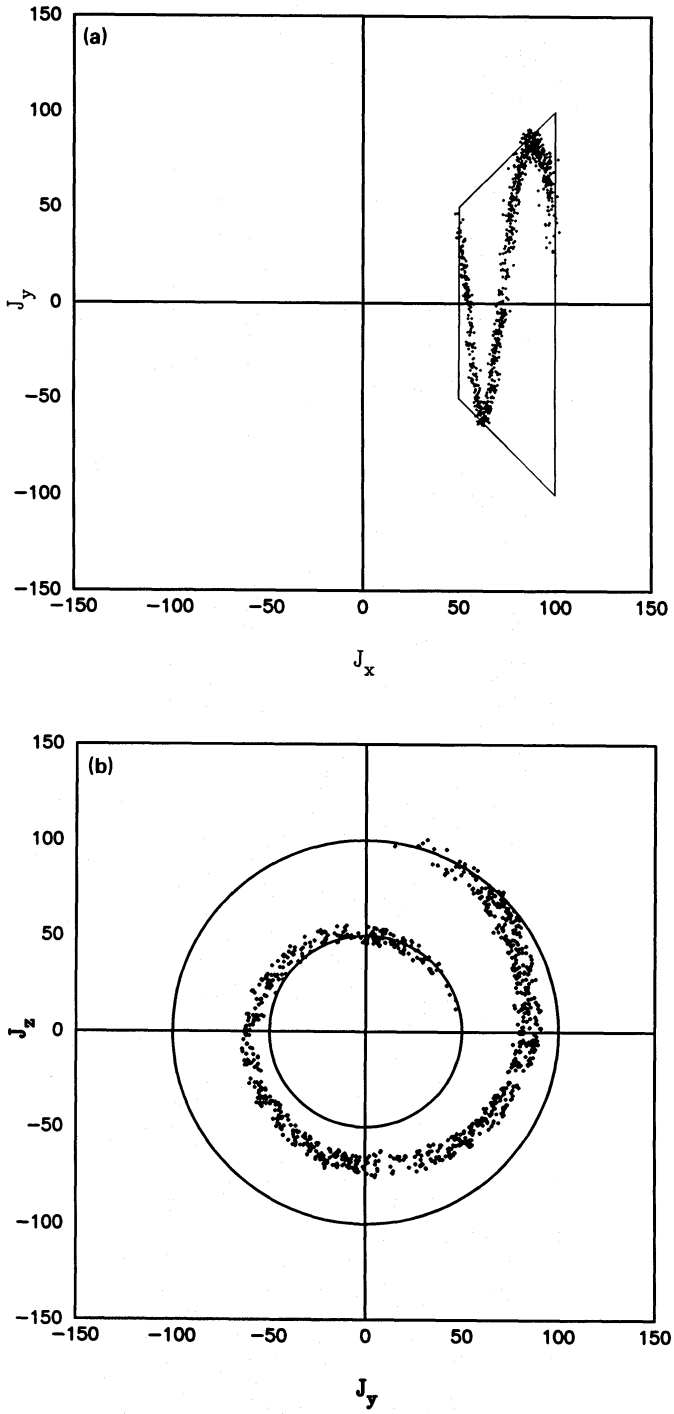

Figure 2. The momentum space positions of 1000 clouds after 1–2 precession times in model O1 projected on to (a) J_x–J_y plane, (b) J_y–J_z plane. The clouds initially filled a disc inclined at $i = 45°$ in the x–z plane, with inner radius 50 units and outer radius 100 units. Each particle moves vertically up and down in Fig. 2(a) on the surface of a truncated cone; they are not confined within the box as the initial disc had a finite thickness. Note the spread in the position of the node of each particle at a given radius.

The orientation of the initial disc is best defined by its total momentum vector $\boldsymbol{J}$. We take $\boldsymbol{J}$ to lie in the x–z plane unless otherwise stated and use the angle, i, that $\boldsymbol{J}$ makes with the z-axis to distinguish our models. From Section 2.3 we expect that small i should lead to long-axis rings whilst large i (close to 90°) should lead to short-axis rings.

3.2 Dissipationless results

As a further test we ran the code without collisions. Particles at different initial radii precessed freely at different rates (precession rate $\propto r$) each moving independently to fill its tube orbit. The available momentum space for model O1 is shown by the truncated cone in Fig. 2. Each cloud moves vertically up and down in Fig. 2(a) but at a different rate at each radius. Thus the initial disc, which would appear as a straight line in this plot, then wraps around the surface of the cone. One important thing to note is that deviations from spherical geometry lead to a small radial excursions and hence a spread in precession times at a given radius. This is crucial for the dissipation mechanism, discussed below.

In the triaxial case the geometry of the orbits is similar except that the boundaries of the available momentum space regions have curved sides because momentum is not exactly conserved along the axis about which the disc is precessing.

3.3 Results with collision algorithm C1

With a cloud radius of 0.5 very few collisions occur (of order 1 per orbit per cloud). This is too few to couple the inner and outer edges of the disc together so the disc rapidly disperses and the momentum space plots 'wind up' as in free precession case above.

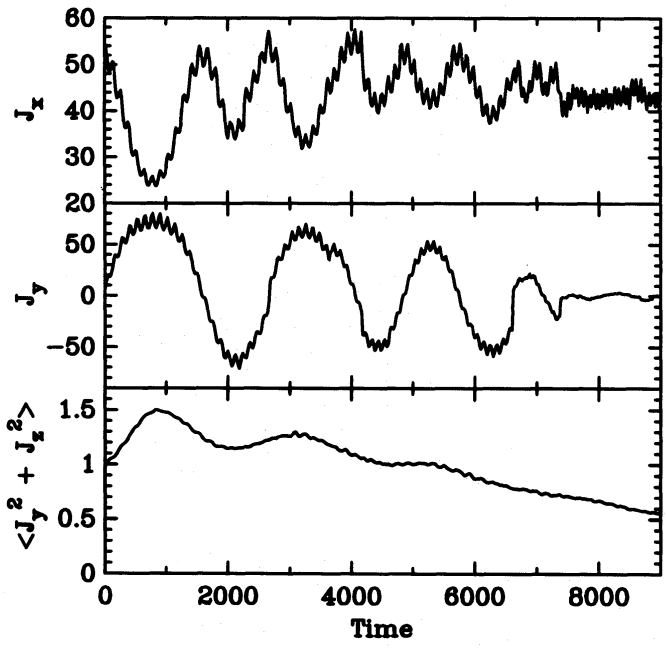

Figure 3. This figure shows results from model T1 with an initial disc configuration as described in Fig. 2. The upper two panels show the angular momenta J_x and J_y for a single sample particle. J_z is similar to J_y (except $\pi/2$ out of phase). The bottom panel contains the sum of $J_y^2+J_z^2$ for all the clouds, normalized to unity initially (a cloud orbiting in the preferred plane would contribute nothing to this total).

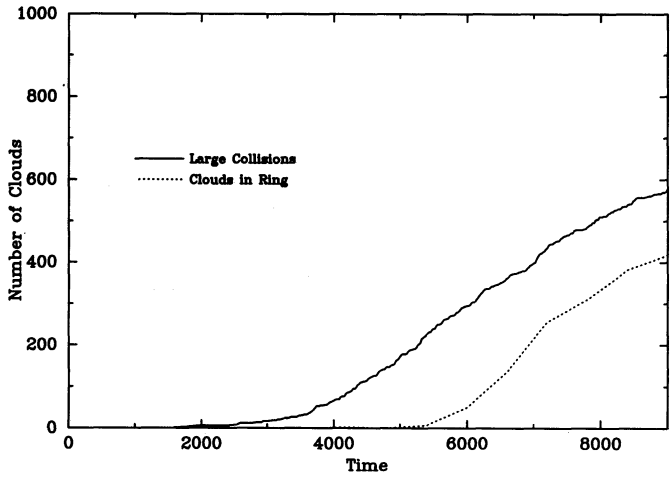

Figure 4. A comparison of the number of clouds which have undergone major collisions in which more than 50 per cent of their momentum perpendicular to the preferred plane was lost and the number of clouds with orbital planes inclined less than 10° away from the preferred plane. The model is described in Fig. 3.

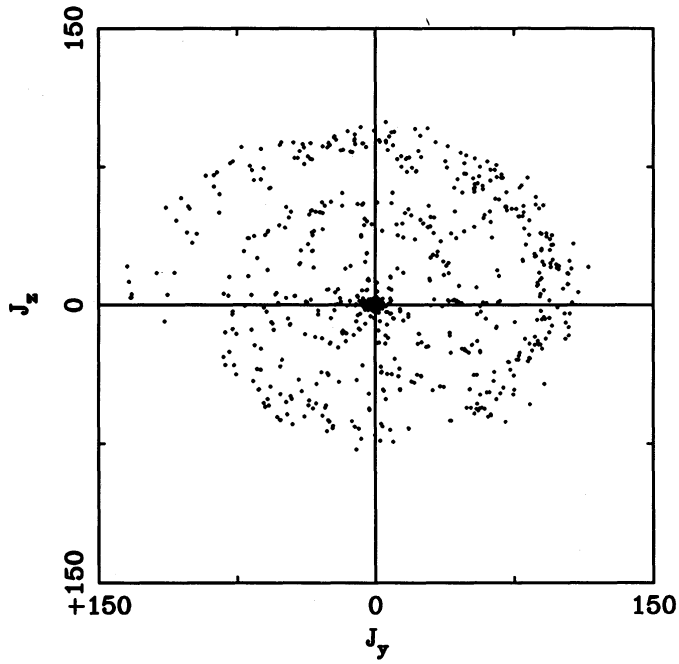

Figure 5. The angular momenta of the 1000 clouds projected on to the J_y–J_z plane at $t=9000$. The model is described in Fig. 3. The large clump of clouds at the origin confirms the presence of a ring in the preferred plane.

As the system evolves so the spread in precession angle, $\Delta\Omega$, at a given radius increases. Once $\Delta\Omega$ equals 180°, collisions can occur between clouds moving in opposite senses relative to the preferred plane. These tend to cancel out the inclined components of the angular momentum and leave the resulting structure orbiting in (or near) the preferred plane. This forms an overdensity of clouds in the plane which other clouds must transit on their orbits; further collisions then lead to the formation of a stable ring.

The main difference between algorithms *C1a* and *C1b* is in the final ring structure. Using *C1a* most of the ring material

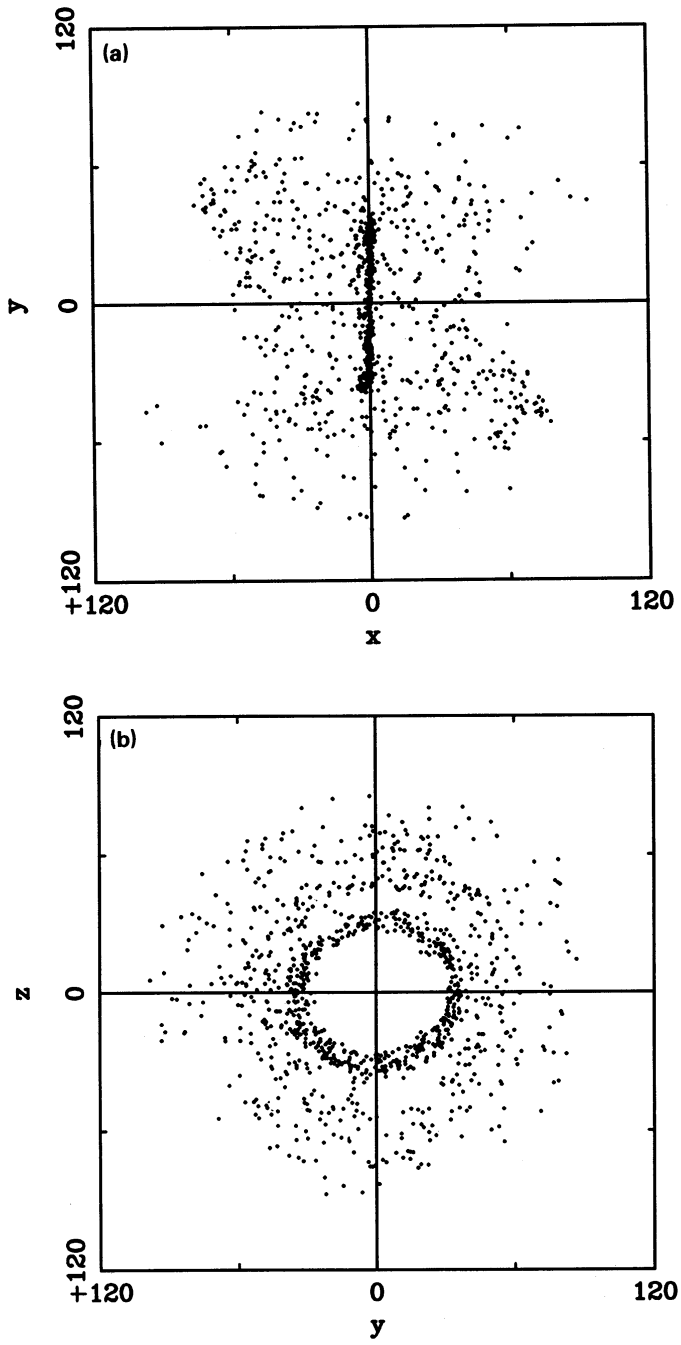

Figure 6. The position of the clouds at the same time as Fig. 5 projected on to (a) the x–y plane, (b) the y–z plane. The model is described in Fig. 3. The map in the x–z plane looks very similar to Fig. 6(a).

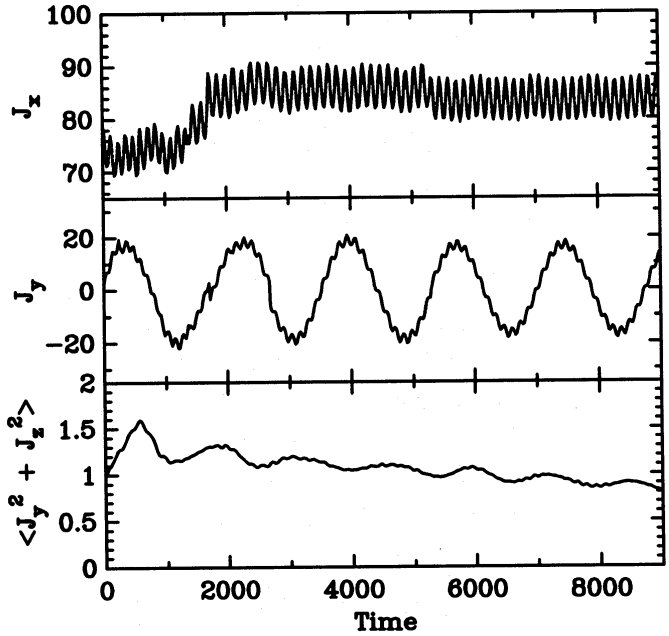

Figure 7. As for Fig. 3, except that the initial disc was inclined at $i = 80°$. Little dissipation has taken place.

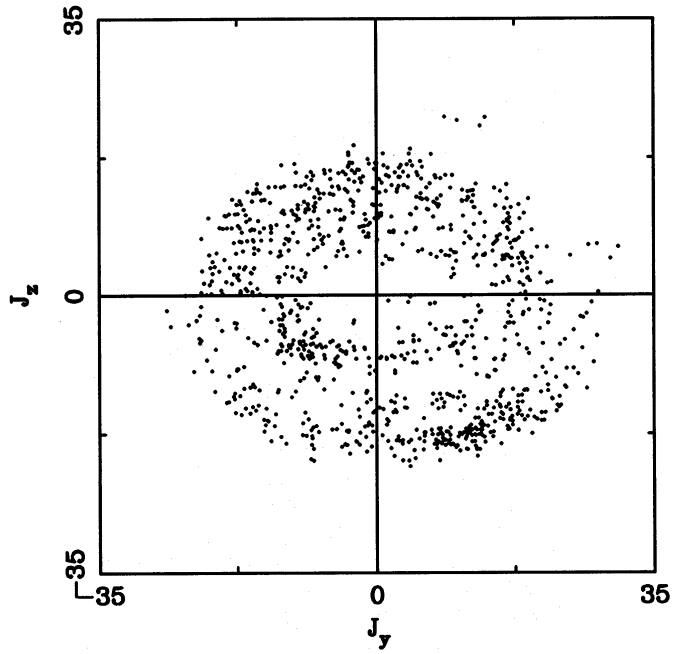

Figure 8. As for Fig. 5 except that $i = 80°$. The lack of any clouds near the origin confirms that no ring has yet formed.

accretes into a few massive clouds, whereas *C1b* gives a relatively uniform distribution as is observed. Both models dissipate at approximately the same rate to begin with but at later times algorithm *C1a* is less efficient as the more massive clouds have a smaller specific cross-section. We use *C1b* as default below.

We first consider the triaxial model T1 with an initial inclination for the annulus of $i = 45°$. Ring formation is best illustrated by Fig. 3 which shows the variation of the angular momentum of single particle, and of the mean angular momentum in the preferred plane, with time. The particle suffers about half a dozen major collisions which tend to reduce its angular momentum perpendicular to the precession axis. The final collision, which occurs after approximately three precession times, brings the particle into the preferred plane. In Fig. 4 we show a number of particles which have undergone a collision that removes more than half of their angular momentum in the plane. Some such collisions occur early-on when the inner regions have differentially precessed by 60° ($\Omega \sim 270°$). Also shown are the number of particles whose angular momentum vector lies within 10° of the precession axis. The rise here occurs later, approximately corresponding to $\Delta\Omega = 180°$. The ring begins to appear soon after, at first tilted a few degrees to the

precession axis but quickly settling down through further collisions into the plane. The components of angular momenta perpendicular to the precession axis and projections of the ring at time 9000 are given in Figs 5, 6(a) and 6(b). Translating to typical real units this snapshot is taken about 3×10^9 yr after the start.

In the oblate potential, O1, ring formation takes much longer because it takes a long time for clouds at the same radii to precess to 180° out of phase. This is because the particles are on almost circular orbits and therefore have a narrow scatter in momentum space (compare the orbital variation shown in Fig. 2(b) with that seen in the upper panel of Fig. 3). The same effect is seen in model T1 for initial discs which lie close to a preferred plane; with $i = 80°$ the particles fill a large fraction of the tube orbit at the endpoint of the integration (~ 50 orbits, ~ 5 precession times at $r \sim$ 50) but not real ring has been formed. The positions and angular momenta at this stage are shown in Figs 7–9; as can be seen there is no collapse to J_y, $J_z \approx 0$ although at small starting angles the position space map always looks like a ring, albeit much thicker than one formed by collisions in the plane. We are thus in the paradoxical situation that initially highly inclined discs form rings much faster than those initially much closer to the desired endpoint and that rapid ring formation only occurs in the more messy triaxial potential.

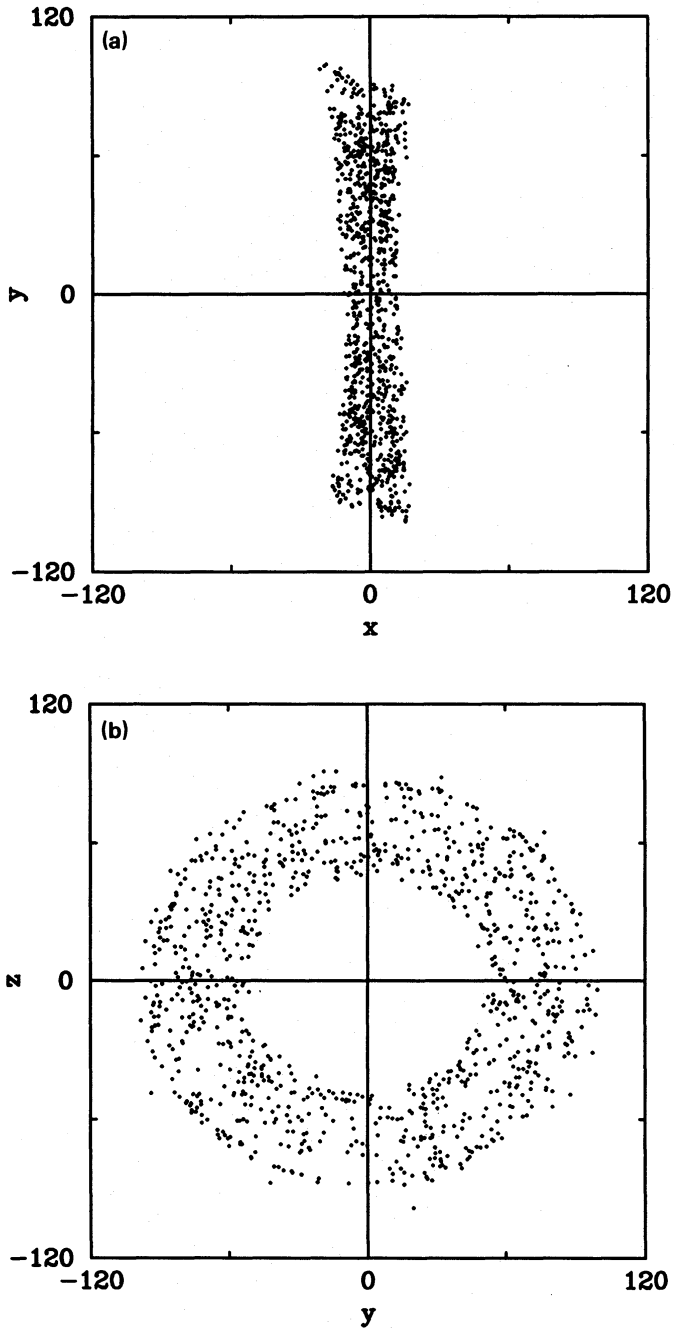

Figure 9. (a) and (b) As for Fig. 6(a) and (b) except that $i = 80°$.

3.4 Results with collision algorithm C2

The above results are qualitatively different from those of HI85 and SD88 who, while noting the process of differential precession, stress cases in which the disc maintains a sheet-like, albeit highly warped, structure. In their models local viscosity acts so as to return the disc to a plane. In our models too dissipation of relative motion does occur, as can be seen in Fig. 7, but this is insufficient to prevent disruption of the disc which requires effective coupling between gas clouds. Even using algorithm **C2** with a narrow radial extent and an inclination angle of less than 10° from a preferred plane we still find it difficult to make the disc precess as a whole.

One should ask whether a larger viscosity can be obtained by varying our model parameters. Increasing the cloud numbers would give a smaller mean-free path and hence more collisions. However, if the mean-free path is made too small then radial excursions are reduced, coupling between different parts of the disc decreases and the viscosity will fall. A large number of clouds would also raise the integration

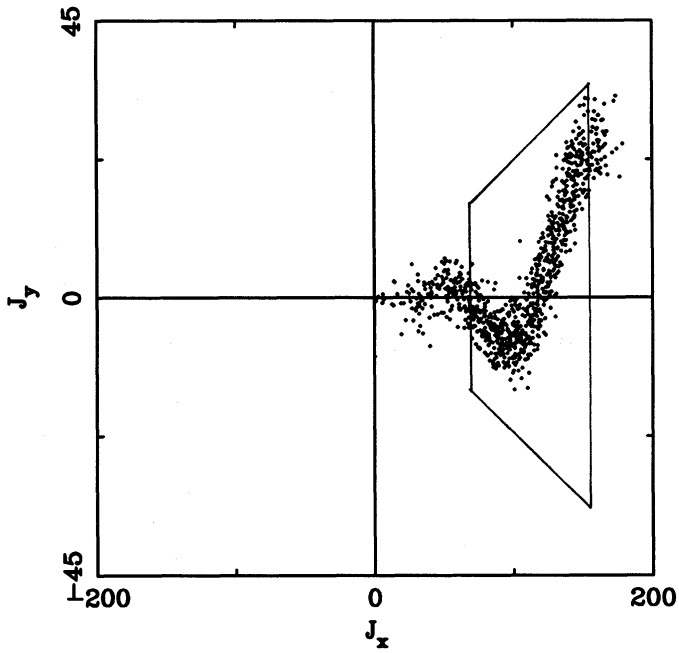

Figure 10. Projected momenta at $t = 3600$ for a disc initially inclined at $i = 80°$ in model T1, using collision algorithm **C2** with $d_{sep} = 6$. The y-axis has been rescaled to aid viewing and a box added to show the available momentum space. Despite the numerical effects seen at the inner and outer edges of the disc, significant damping does appear to have occurred (*cf.* Fig. 2a).

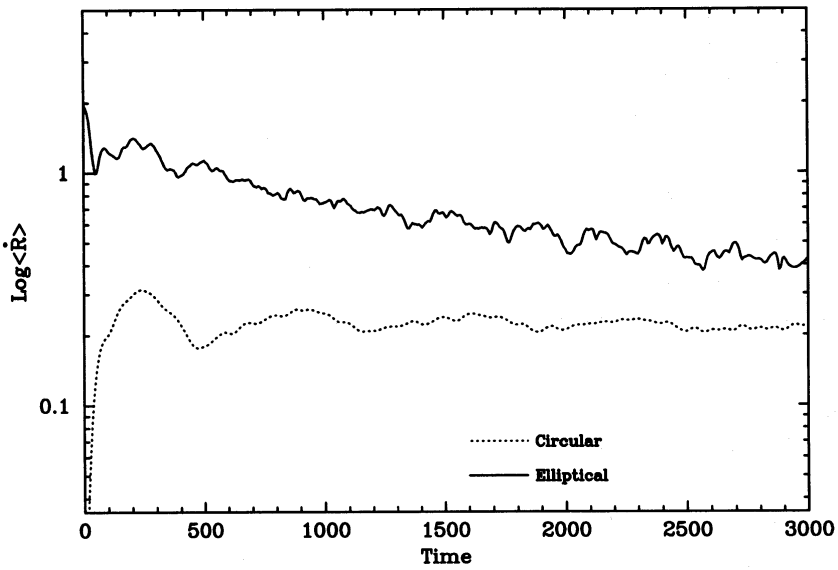

Figure 11. Comparison of $\langle \dot{r} \rangle$ for model O1 between clouds initially moving on circular and elliptical orbits. The circular orbits rapidly acquire a radial component from the potential whilst the elliptical orbits lose their eccentricity by cloud–cloud collision.

time of our code unacceptably. Instead we choose to artificially increase the range over which viscosity acts by using collision algorithm **C2** applied to model T1 with $i = 80°$. The damping rate is very dependent on the dissipation range, d_{sep}. With $d_{sep} = 2.5$ (similar to the direct collision range) and $d_{sep} = 4.0$ no rapid damping occurs and the results look just like those for free precession. Using $d_{sep} = 6.0$ the inclination of the inner regions of the disc does appear to decrease substantially before differential precession is effective (Fig. 10), however, spurious numerical artefacts begin to appear. These completely dominate for $d_{sep} = 10.0$ which is not surprising as this is a significant fraction of the size of the disc. As our code stands the clouds tend to spiral into the centre from the inside of the ring as the one nearer the middle constantly loses energy, and, because we only choose to dissipate convergent motions, clouds tend to move as far apart as possible and remain there.

It is difficult to disentangle these numerical artefacts from the dissipation mechanism we are trying to model. Perhaps turbulence in a continuous gas distribution would lead to long-range interactions of this kind. The smoothing kernel used by HI85 in their smooth-particle hydrodynamics, which is Gaussian of rms 250 pc (2.5 units) will give interactions over a similar length scale of 500 pc or more. Because some dissipation from collisions of particle on neighbouring orbits is seen to occur, and because this is expected to increase at small inclinations, it does seem possible that this approach can lead to ring formation in the desired plane for the restricted class of initial conditions involving a slightly inclined narrow disc. However, extreme parameters, $d_{sep} \gtrsim 500$ pc and $i \leq 10°$ seem to be required. For this reason we prefer to treat the gas as a system of isolated clouds as in *C1b*.

3.5 Conclusions

We have shown that ring formation is caused by differential precession of particles (gas clouds) in a non-spherical potential. Either strong dissipation of relative motions may lead to precession of the disc as a whole or, more likely, particles precess freely until their orbits intersect those moving the other way through the preferred plane. In the latter case differential precession must give a relative phase shift of 180° *at the same radius*. The time for this to occur is decreased in triaxial potentials or with elliptical or non-planar initial conditions and agrees well with theoretical estimates. Any disc formation scenario is likely to involve an untidy collision between the primary and gas-rich spiral or irregular companion. The gas will not be injected into the system in a smooth, cold disc and so it is not clear that whole-disc precession can occur. On the other hand differential precession of gas clouds will be enhanced. We consider realistic initial conditions in the next section.

4 RING FORMATION

4.1 Radial motions

As a first step towards realistic initial conditions (approximating those occurring during gas infall or the disruption of a gas-rich secondary galaxy) we examine ring formation from an initially flat disc within which the clouds are moving on non-circular orbits. Each cloud's initial position and speed within the disc are generated exactly as before, but the velocity vector is then rotated in the plane of the orbit through an angle chosen uniformly between $\pm 60°$. The starting disc thus has clouds moving on eccentric orbits with random nodes and phases.

Collisions are initially very frequent and tend to circularize the orbits. This process cannot proceed to completion due to differential precession of the orbits, however, the residual radial motions are small. Fig. 11 shows the evolution of the rms value of $\dot{r}$ with time for initially elliptical and circular orbits in potential O1. The non-spherical gravitational potential quickly induces small radial excursions in the circular orbits, which are important for damping of the disc as described in Section 3. Most of the radial parts of the elliptical orbits are rapidly destroyed and

after approximately a precession time these are reduced to just twice the circular case. These results suggest, and are borne out by the more complicated starting conditions below, that ring formation takes place in the same manner and at almost the same rate regardless of the initial radial motions. These are quickly dissipated and if anything tend to reduce the disc width by bringing the inner and outer regions into contact. There may be an associated reduction in the orbital radii as the angular momentum is smaller than for circular motions.

4.2 Merger of a secondary

In this section we roughly approximate the initial conditions of 1000 gas clouds after the disruption of a gas-rich secondary galaxy. We take a radius of 12 units and a full disc-height of 4 units for our secondary, approximating the axis ratios of a dwarf spiral of radius 1200 pc and height 400 pc. The initial conditions in the disc of the secondary were generated in the same manner as in Section 3.1 but with a circular velocity of 0.5 units and an inner radius of 2 units to prevent confusion of the results from clouds on highly inclined orbits. Thus we envisage a collision between a gas-rich dwarf spiral of mass $\sim 10^9\ M_\odot$ and a giant elliptical of mass $\sim 10^{11}\ M_\odot$.

Following Quinn (1984) we assume that the secondary is completely unaffected by the primary until the tidal force is sufficient to overcome the internal gravity at its edge (12 units). At this point we assume complete disruption and the subsequent evolution of the cloud orbits is determined only by the gravity of the primary. Possible drawbacks of this approach were discussed by Quinn (1984). It is possible to overestimate the velocity spread of the clouds since the energy of escape from the secondary is neglected and this can help to 'puff up' the height of the proto-ring. On the other hand the spread in position is underestimated as gas clouds will in reality be stripped from the secondary at many points along its orbit. A more detailed simulation of the collision is necessary to generate accurate initial conditions but the simple case considered here should mimic the generic behaviour.

Quinn's study relates to head-on collisions which for our model simply lead to a large conglomeration of clouds at the centre of the primary. We are more interested in glancing collisions and take the distance of closest approach to be 60 units (which is about the tidal radius). The orbital velocity of the secondary is set equal to the circular velocity. Immediately after disruption each cloud moves off with a velocity that is the resultant of its rotation velocity within the secondary and the collision velocity.

4.3 Ring formation after merger

The subsequent evolution of the system follows two different routes depending upon the inclination of the plane of the secondary relative to the position and direction of its orbit about the primary. If the disc's angular momentum vector is approximately aligned (or anti-aligned) with the collision direction then the clouds from a thin rope-like structure (Fig. 12) because they occupy a small volume in phase space: they all start with approximately the same position and orbital velocity. If the rope-like structure closes upon itself then cloud–cloud collisions rapidly form a narrow circular disc inclined at the same angle as the initial collision inclination of the secondary. After this the system evolves in the same way as described in Section 3.3, though because of the small range of radii dissipation from particles on neighbouring orbits it is increased and so is the break-up time of the disc (see Fig. 13).

Alternatively, if the disc's angular momentum vector is more than about 30° away from the collision direction then a rope-like structure does not form and the clouds rapidly spray out to fill the available tube orbit (Fig. 14). No well-defined structure is evident until a single precession time has elapsed and then a ring rapidly forms near to the preferrred plane (Fig. 15). Because of the non-uniform distribution of gas clouds and the speed with which the tube orbit is filled there is not an even distribution of clouds above and below the preferred plane. For this reason the ring need not form exactly in a preferred plane but can be tilted by a few degrees. The inclination increases as the change over between the rapid filling of the tube orbit and the rope-like structures is approached. One example of a borderline case which we ran formed a ring inclined at about 20° to the preferred plane from initial impact planes inclined at 45°.

5 DISCUSSION

5.1 The shape of the potential

Our simulations do not add much to previous investigations of the shape of the potential because the capture rate into polar orbits is the same. We note that triaxial potentials encourage dissipation by inducing radial motions. The general concensus in the literature is that the host galaxy is an oblate S0 rather than a tumbling prolate system (e.g. SWR, WMS) with the main evidence being the large ratio of rotation speed to velocity dispersion. For polar orbits to be stable, however, we require that the potential be prolate or triaxial with even moderate degrees of triaxiality giving substantial capture cross-sections (SD82). Recent numerical results (Allen, Palmer & Papaloizou 1990; Palmer, Papaloizou & Allen 1990) suggest that in many circumstances the triaxial state may be the only stable configuration of an elliptical galaxy. Direct evidence is given by the stability of two perpendicular rings as seems to be the case in NGC 2685 and ESO 474 − 626. Also, if Hoag-type objects are face-on polar rings then the central galaxies exhibit a wide range of flattenings (Wakamatsu 1990) which are more indicative of triaxial hosts rather than central discs.

5.2 Accretion into the galactic core

HI85 suggest that the loss of angular momentum through dissipation could lead to gas infall into the core of the host galaxy and give two ways in which this might come about. If we consider the dissipation of radial motions in a ring then the rate of energy loss is of order $\frac{1}{2}(\Delta\dot{r})^2$ per orbit, where the induced radial motion due to the non-spherical potential $\Delta\dot{r} \sim v_c(\Delta r/r)$. From our simulations $\Delta r/r \approx 0.1$, i.e. of the same order as the deviations from sphericity of the galactic potential. As the gas clouds spiral in to the centre of the galaxy their orbits will remain circular with an orbital speed equal to $\sqrt{2}$. If we equate the loss of energy to the change in potential energy of the orbit then the number of orbits

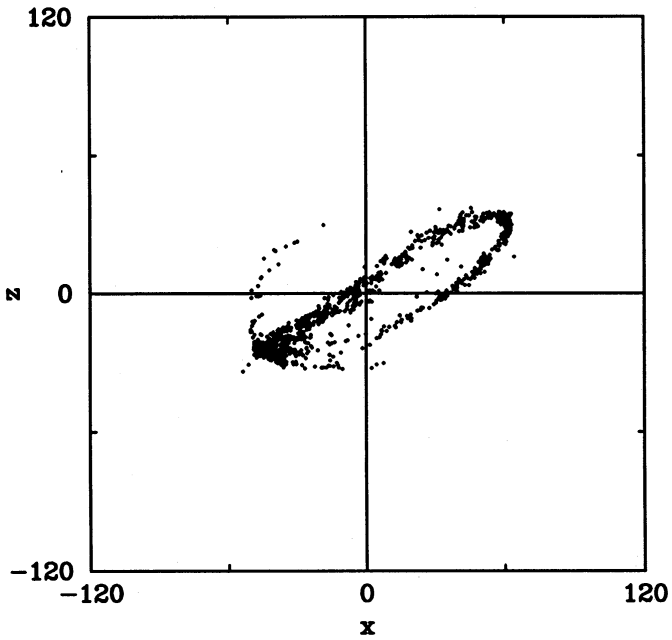

Figure 12. Evolution of the gas clouds after a secondary was disrupted in model T1 at $(x, y, z) = (0, 42, 42)$ with collision velocity $(v_x, v_y, v_z) = (\sqrt{2}, 0, 0)$ and rotational angular momentum aligned with the collision direction. The projected cloud positions in the x–z plane are shown at $t = 600$ when a thin rope-like structure has formed.

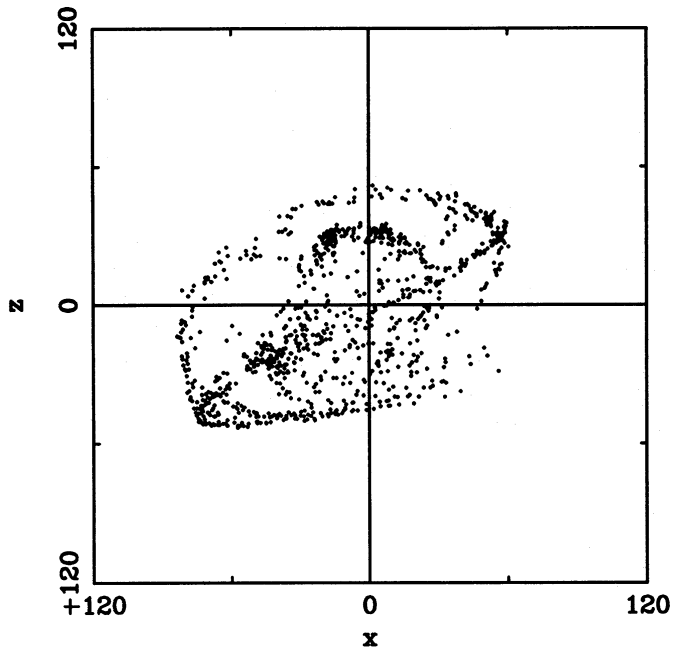

Figure 14. As for Fig. 12 except that the rotational angular momentum was in the y direction, 90° away from the direction of the orbital motion. The clouds are already close to filling the available position space.

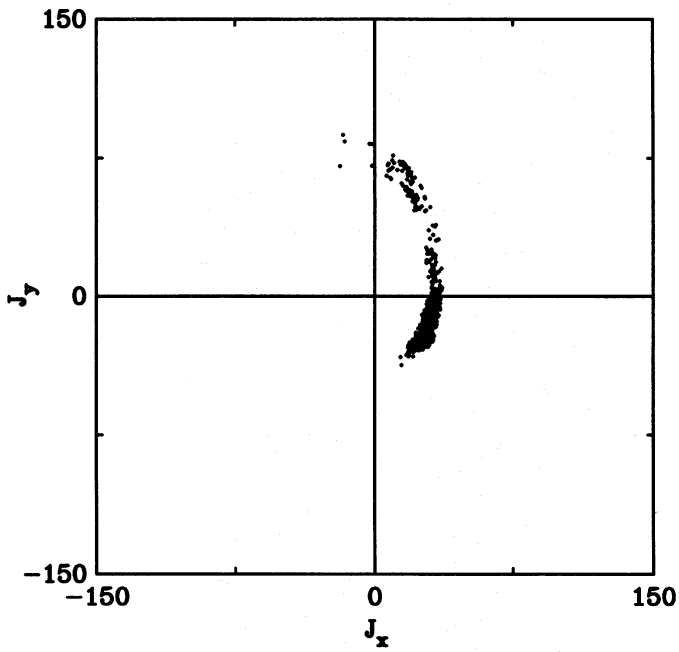

Figure 13. The projection of the cloud momenta in the J_x–J_y plane for the model described in Fig. 12 at $t = 3000$.

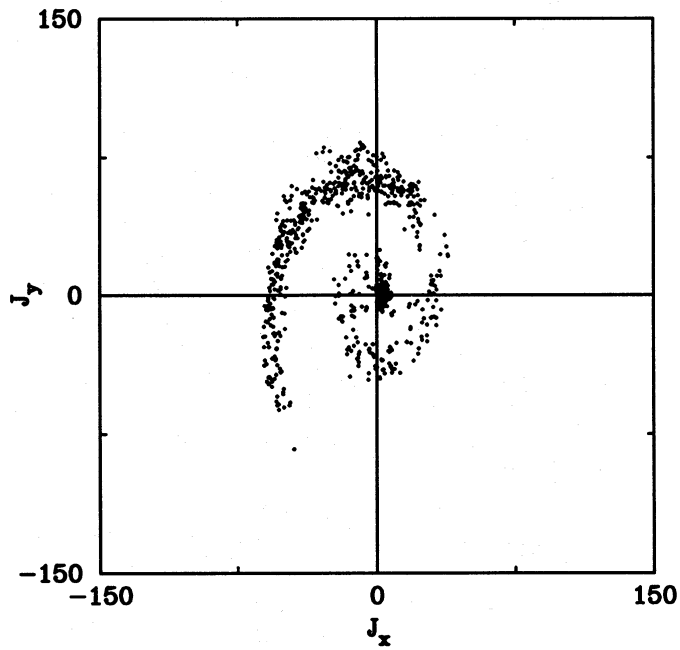

Figure 15. As for Fig. 13 but for the model described in Fig. 14. The large clump of clouds near the origin confirms the presence of a ring close to the preferred plane (*cf.* Fig. 5).

required to move in a factor of two in radius is $N \sim 2 \ln 2/(0.1)^2 \sim 140$. At $r = 100$ (~ 10 kpc) the orbital period is approximately 10^8 yr and so it takes a Hubble time for gas to move in by a significant fraction of its radius. The decay rate will be faster at smaller radii but note that our estimate is a maximum assuming perfect dissipation of all the induced radial motions. It seems that infall through dissipation in a smooth disc can only be important within the core of the galaxy and that the observed polar rings are stable in this respect.

However, many of our simulations (and those of HI85) do show accumulation of gas near the centre of the galaxy – these are runs in which angular momentum is lost through collisions of gas clouds on widely differing orbits. When gas clouds have precessed through $\Delta\Omega = 180°$ they then collide to form an annulus whose inner and outer radii are equal to the projection of the initial disc radii along the precession

axis. In addition the gas clouds loose much of their angular momentum and will undergo further collisions in the stable plane; and (iii) formation of a tilted disc which then undergoes Thus for an initial disc inclined at an angle i to the precession axis the orbital radius decreases by a factor of $\cos^2 i$. We note that many observed ring systems show enhanced star formation at their inner edges as would be expected in this scenario. The reduction in radius is greatest for axisymmetric potentials where high inclinations, $i \sim 90°$, albeit with correspondingly long precession times, can be achieved. Unfortunately, even a moderate degree of triaxiality can limit $\cos i$ to be greater than ~ 0.5 (SD82). This discussion applies equally well to whole-disc precession.

A third mechanism shows up in our simulations. The most dramatic influx of gas into the galactic core comes when gas clouds are able to precess around both the major and minor axes as there is then no component of systemic angular momentum which is even approximately conserved. Typically we find that a ring forming in the plane perpendicular to one precession axis is rapidly destroyed by collisions with clouds precessing around the other. The orbits in the inner regions appear chaotic and clouds appear in the core soon thereafter. In fact we had great difficulty in producing examples of galaxies with two perpendicular rings. It is possible that two distinct accretion events, or a single merger in which gas is stripped of the secondary over a wide range of radii, might have the desired effect. However, detailed modelling of the accretion process is required to show that the inner ring could survive. Alternatively the host potential might be almost axisymmetric in which case the inner ring would form well inside the orbits of the outer particles, however, we have been unable to produce this effect in our simulations.

5.3 Ring formation mechanism

We have identified at least three different modes of stable ring formation: (i) direct formation of a ring in a preferred plane following a chaotic collision; (ii) initial formation of a tilted disc which then breaks up and later reforms in the plane; and (iii) formation of a tilted disc which then undergoes solid body precession down into the plane. The first two of these mechanisms have been demonstrated in our simulations; the third was claimed by HI85 but was not clearly reproducible by us. Mechanism (i) is quite rapid, the other two, by effectively dissipating the initial radial motions, take a differential precession time for the gas at a given radius, which is much longer. In addition, there is a further possibility (iv) that all polar rings are really transient discs, forming in the collision plane, then breaking up through differential precession never to reform.

Our simulations follow the dynamics of gas clouds, however, it is young stars which dominate the observational selection of polar rings. If we suppose that star formation is triggered by intercloud collisions then each of the formation scenarios will give different signatures: the first should never lead to rings at high inclination angles, however, IIZw73 appears to be one (but the only) clear-cut example (Whitmore 1984) – so at least some collisions must produce tilted rings. On the other hand mode (iii) would give rings at a whole range of inclinations, and since the dissipation time is of order a Hubble time, we should expect many of them to still be observable. It could be argued that (iv) fits the observations as near-polar rings in oblate potentials are slowly precessing and would survive longer than those at higher inclinations. A detailed statistical study of the observed inclinations would be necessary to test this.

The H I radio observations do not add to the statistics as they are usually undertaken on optically selected candidate polar ring galaxies; were there to be a lot of fragmented rings, as in (ii) for example, these would not be detected. The gas content is poorly resolved but does generally align with that of the optical ring, often with greater extent (van Gorkom *et al.* 1987). There is at least one example, ESO 415 – G 26, where the weaker hydrogen contours outline a butterfly shape reminiscent of the broken disc seen in Fig. 6(a). In general the stellar ring lies at the inner edge of the H I region, as expected in models (i) and (ii) where the collision in the preferred plane leads to a loss of orbital angular momentum and hence a decrease in radius. However, this evidence is ambiguous because, even in a long-lived disc, collisions, and hence star formation, would be more frequent near the centre.

Apart from the presence of young stars, there are secondary indications that many of the observed polar ring systems are young. Balmer absorption in the nucleus of NGC 4650A is indicative of a recent merger as are the irregular shell-like structures seen in many others (WMS). If the ages are typically less than a few orbital periods then the scarcity of highly inclined rings would seem to rule out model (ii).

Our favoured mechanism is therefore formation of polar rings in or close to a preferred plane, perhaps with a short-lived initial highly inclined disc formed immediately after the collision.

ACKNOWLEDGMENTS

We are extremely grateful to Scott Tremaine for suggesting this project and for many useful suggestions along the way. Thanks also to the referee whose comments helped to clarify some of the text. FRP was supported by a SERC studentship.

REFERENCES

Allen, A. J., Palmer, P. L. & Papaloizou, J., 1990. *Mon. Not. R. astr. Soc.*, **242,** 576.
Athanassoula, E. & Bosma, A., 1985. *Ann. Rev. Astr. Astrophys.*, **23,** 147.
Binney, J. & Tremaine, S., 1987. *Galactic Dynamics,* Princeton Series in Astrophysics.
Brinks, E. & Burton, W. B., 1983. *The Milky Way Galaxy, IAU Symp. No. 106,* Reidel, Dordrecht, Holland.
Dobrovolski, A. R., 1980. *Icarus,* **43,** 222.
Durisen, R. H., Tohline, J. E., Burns, J. A., Dobrovolski, A. R., 1983. *Astrophys. J.*, **264,** 392.
Goldstein, H., 1980. *Classical Mechanics* 2nd edn, Addison-Wesley World Student Series.
Habe, A. & Ikeuchi, S., 1985. *Astrophys. J.*, **289,** 540.
Hoag, A. A., 1950. *Astr. J.*, **55,** 170.
Mould, J., Balick, B., Bothun, G. & Aaronson, M., 1982. *Astrophys. J.*, **260,** L37.
Palmer, P. L., Papaloizou, J. & Allen, A. J., 1990. *Mon. Not. R. astr. Soc.*, **243,** 282.
Quinn, P. J., 1984. *Astrophys. J.*, **279,** 596.

Schweizer, F., Ford, W. K., Jedrzejewski, R. & Giovanelli, R., 1987. *Astrophys. J.*, **320,** 454.
Schweizer, F., Whitmore, B. C. & Rubin, V. C., 1983. *Astr. J.*, **88,** 909.
Shane, W. W., 1989. *Astr. Astrophys.*, **82,** 314.
Steinman-Cameron, T. Y. & Durisen, R. H., 1982. *Astrophys. J.*, **263,** L51.
Steinman-Cameron, T. Y. & Durisen, R. H., 1984. *Astrophys. J.*, **276,** 101.
Steinman-Cameron, T. Y. & Durisen, R. H., 1988. *Astrophys. J.*, **325,** 26.
Taniguchi, Y., Shibata, K., Wakamatsu, K., 1986. *Astrophys. Space Sci.*, **118,** 529.
Tenorio- Tagle, G., 1990. *Large-scale propagating star formation and the physics of self-regulation,* Max-Planck Institut fur Astrophysik, West Germany, preprint.
Tohline, J. E. & Durisen, R. H., 1982. *Astrophys. J.*, **257,** 94.
Tohline, J. E., Simonson, G. F. & Caldwell, N., 1982. *Astrophys. J.*, **252,** 92.
van Gorkom, J. H., Schechter, P. L. & Kristian, J., 1987. *Astrophys. J.*, **314,** 457.
Wakamatsu, K., 1990. *Astrophys. J.*, **348,** 448.
Wakamatsu, K. & Arp, H., 1983. *Astrophys. J.*, **273,** 167.
Whitmore, B. C., 1984. *Astr. J.*, **89,** 618.
Whitmore, B. C., McElroy, D. B. & Schweizer, F., 1987. *Astrophys. J.*, **314,** 434.